

Calorimetric Studies of Melanotransferrin (p97) and Its Interaction with Iron*

Received for publication, December 29, 2004, and in revised form, February 9, 2005
Published, JBC Papers in Press, February 9, 2005, DOI 10.1074/jbc.M414650200

A. Louise Creagh‡, Jacqueline W. C. Tiong§, Mei Mei Tian§, Charles A. Haynes‡¶, and Wilfred A. Jefferies¶¶**‡‡

From the ¶Michael Smith Laboratories and §Biomedical Research Centre, Department of Microbiology and Immunology and the Departments of ¶Zoology, **Medical Genetics, and ‡Chemical and Biological Engineering, University of British Columbia, Vancouver, British Columbia V6T 1Z4, Canada

The mammalian molecule melanotransferrin (mTf), also called p97, is a member of the transferrin family of molecules. It exists in both secreted and glycosylphosphatidylinositol-anchored forms and is thought to play a role in angiogenesis and in transporting iron across the blood brain barrier. The binding affinity of iron to this molecule has not been formally established. Here, the binding of ferric ion (chelated with a 2-fold molar ratio of nitrilotriacetate) to mTf has been studied using isothermal titration calorimetry and differential scanning calorimetry. One iron-binding site was determined for mTf with similar binding characteristics to other transferrins. In the absence of bicarbonate, binding occurs quickly with an apparent association constant of $2.6 \times 10^7 \text{ M}^{-1}$ at 25 °C. The presence of bicarbonate introduces kinetic effects that prevent direct determination of the apparent binding constant by isothermal titration calorimetry. Differential scanning calorimetry thermograms of mTf unfolding in the presence and absence of iron were therefore used to determine the apparent binding constant in the bicarbonate-containing system; at pH 7.5 and 25 °C, iron binding occurs in a 1:1 ratio with a K_{app} of $4.4 \times 10^{17} \text{ M}^{-1}$. This affinity is intermediate between the high and low affinity lobes of transferrin and suggests that mTf is likely to play a significant role in iron transport where the high affinity lobe of transferrin is occupied or where transferrin is in proportionally low concentrations.

Iron is an essential element for the vast majority of organisms on the planet (1, 2). Recent studies on the divalent metal transporter DMT-1 (also known as Nramp2), the iron-regulated transporter IREG-1 (also known as ferroportin or MTP1), transferrin receptor 2, and iron-regulated ferric reductase have greatly improved our understanding of iron metabolism in many species (3–5). However, the best studied iron uptake system remains the classical transferrin/transferrin receptor (Tf/TfR)¹ system. Diferric-loaded Tf binds to the TfR on the cell surface. The Tf/TfR complex is then internalized through the

clathrin-mediated endocytosis pathway. Once inside the cell, the clathrin-coated vesicles either fuse with or mature into endosomes. The decrease in endosomal pH results in a decrease in the affinity of iron for the Tf/TfR complex. The free iron is then translocated into the cytoplasm. This process is mediated by a 12-membrane-spanning metal transporter known as Nramp2 (4). Iron is thought to be incorporated into the iron storage protein, ferritin, in the cytoplasm. Whether this incorporation is mediated by a chaperone protein or by another process remains unknown. Recent structural studies have substantially revised our understanding of this process. The binding of Tf to TfR results in a conformational change in Tf and substantially hinders the iron release from its high affinity N lobe. One scenario therefore suggested by this finding is that the atom of iron bound to the low affinity C lobe is exclusively released during each cycle of internalization of the Tf/TfR complex (6).

There exist other iron uptake pathways that are independent of Tf (1, 7). One of these pathways is mediated by melanotransferrin (also referred to as p97 or mTf). It is a 97-kDa protein belonging to the Tf family, which includes serum Tf, lactoferrin, and ovotransferrin. It shares a 40% sequence identity with human lactoferrin (8). Melanotransferrin was first identified as a cell surface marker for human skin cancer (9). However, the protein was subsequently found to be expressed at various levels in the liver, intestine, umbilical cord, placenta, sweat gland, and more recently in human brain endothelium (10). It has also been shown to be relatively conserved across various species (11). Unlike the other members of the Tf family, mTf exists in two different isoforms as a result of alternate splicing of the mRNA (11). It can be found as a membrane protein attached to the cell surface via a glycosylphosphatidylinositol (GPI) anchor or as a soluble form in serum (12, 13). Our research has recently shown that soluble mTf loaded with iron crosses the blood-brain barrier (14). Iron binding studies on a TfR-deficient Chinese hamster ovary cell line transfected with GPI-anchored human mTf show that the iron uptake process is both saturable and temperature-dependent (7); however, little else is known about this process.

mTf is structurally very similar to other transferrins, consisting of two genetically related lobes, the N lobe (residues 20–361) and the C lobe (residues 362–713). Each lobe is comprised of two dissimilar subdomains that form a deep cleft capable of binding a single ferric ion and a synergistic anion, normally bicarbonate, but a number of other small carboxylate anions containing a second electron donor also function synergistically. The iron binding ligands are identical in each lobe of

* The costs of publication of this article were defrayed in part by the payment of page charges. This article must therefore be hereby marked "advertisement" in accordance with 18 U.S.C. Section 1734 solely to indicate this fact.

‡‡ Supported by the Canadian Institute of Health Research. To whom correspondence should be addressed: The Michael Smith Laboratories, 2185 East Mall, The University of British Columbia, Vancouver, BC V6T 1Z3, Canada. Tel.: 604-822-6961; Fax: 604-822-7815; E-mail: wilf@brc.ubc.ca.

¹ The abbreviations used are: Tf/TfR, transferrin/transferrin receptor; mTf, melanotransferrin; GPI, glycosylphosphatidylinositol; ITC, isothermal titration calorimetry; DSC, differential scanning calorimetry; Lf, lactoferrin; oTf, ovo transferrin; hTf, human transferrin; Fe-NTA, iron-nitrilotriacetate.

every transferrin (15); the bound ferric ion is octahedrally coordinated to 4 conserved residues (a histidine, two tyrosines, and an aspartic acid) and to 2 oxygens of the synergistic carbonate ion (15). Examination of the mTf sequence in comparison to the crystal structure of Lf suggests that mTf has an intact transferrin-type iron-binding site in its N lobe. However, it is predicted to have lost the ability to bind iron in its C lobe as a result of several amino acid substitutions (16).

The binding of iron to oTf and hTf has been extensively characterized by spectroscopic and calorimetric techniques (17–21). Comparatively little is known about the thermodynamics of ferric ion binding to mTf. Spectroscopic studies of mTf (22), as well as iron uptake rates into mammalian cells (7), suggest that the protein binds only one ferric ion, in agreement with the putative binding stoichiometry originally proposed by Baker *et al.* (16) based on sequence alignment with hTf and oTf. In this report, we examine the binding characteristics of Fe-NTA to soluble mTf using differential scanning calorimetry (DSC) and isothermal titration calorimetry (ITC) both in the presence and absence of bicarbonate. These experiments establish mTf as a mammalian iron binding molecule capable of delivering iron under physiological conditions.

EXPERIMENTAL PROCEDURES

Materials—The Chinese hamster ovary cell line TRVb receptor (obtained from Dr. F. Maxfield, New York University), which expresses no endogenous hamster transferrin, was transfected with the mTf expression vector pSV2p97a and the G418 resistance vector pWJ218. The pSV2p97a vector (obtained from Dr. G. Plowman and Dr. K. E. Hellström, Bristol-Myers Squibb, Seattle, WA) contains the entire encoding region of mTf driven by the SV40 early promoter. The resulting cell line was designated p97TRVb and maintained in HAM'S F12 medium (Invitrogen) supplemented with 10% fetal calf serum (Invitrogen), 20 mM HEPES, 2 mM L-glutamine, and 500 μ g/ml geneticin (Invitrogen).

The soluble form of mTf was generated by introducing a STOP codon immediately following the glycine residue at position 711, resulting in the protein being devoid of the GPI anchor. Generation of the shortened form of p97 terminating at amino acid position 711 was achieved by PCR utilizing primers WJ67 (5'-GGC ATA AGC TTG GCC CCA GCC AGC CCC GAC GGC GCC-3') and WJ68 (3'-C AGC AGA GTC GTC ACG AGC CCG ACT ATT CGA ATA CGG-5'). The PCR product was cloned into the pNUT vector (R. Palmiter) and transfected into BHK TK⁻ ts13 cells (ATCC CRL 1638). The cells were cultured in Dulbecco's modified Eagle's medium supplemented with 10% fetal calf serum, 20 mM HEPES, 2 mM L-glutamine, and 500 μ M methotrexate (Faulding). The collected supernatant was passed through a column of L235 mAb (ATCC HB8446) immobilized on AfGel10 (Bio-Rad). The mTf protein was eluted off with 0.1 M citric acid, pH 2.5, and subsequently neutralized with 1 M HEPES to pH 7.4 ± 0.4 .

The mTf protein (eluant) was dialyzed for 2 days in 0.2 M KH_2PO_4 , 1 mM EDTA, and 1 mM sodium nitrilotriacetic acid (NTA) in a 10,000 MWCO dialysis cassette (Pierce) at 4 °C with constant stirring. The apo-mTf recovered from the dialysis procedure was subjected to an additional dialysis in 50 mM HEPES overnight at 4 °C. The 50 mM HEPES had been previously prepared by treatment with Chelex-100 (Bio-Rad) to remove any trace metals. All glassware and plastic containers were treated with 4 M HCl for 20 min and rinsed with deionized Millipore water to ensure metal-free conditions. Following dialysis, the apo-mTf protein was concentrated in a Centriprep-30 (Amicon) and its concentration determined spectrophotometrically (280 nm) using an extinction coefficient of $1.214 \text{ (mg/ml)}^{-1} \text{ cm}^{-1}$ ($115,004 \text{ M}^{-1} \text{ cm}^{-1}$).

mTf samples containing iron (for DSC experiments) were prepared by mixing appropriate amounts of protein, buffer, and Fe-NTA stock solution. The Fe-NTA stock solution was prepared by mixing 1 volume of 0.3 M FeCl_3 (in water) with 2 volumes of 0.3 M NTA, disodium salt (in water) and diluting to the appropriate concentration with buffer. Protein solutions, buffers, and solid reagents used for the preparation of bicarbonate-free solutions (for ITC experiments) were stored in a vacuum desiccator containing soda lime.

Isothermal Titration Calorimetry—ITC studies were carried out on a MicroCal MCS-ITC (MicroCal Inc., Northampton, MA); data analysis was performed using software (Origin) supplied by MicroCal. All experiments were carried out in 100 mM Hepes, pH 7.5 ± 0.2 (the pH of each

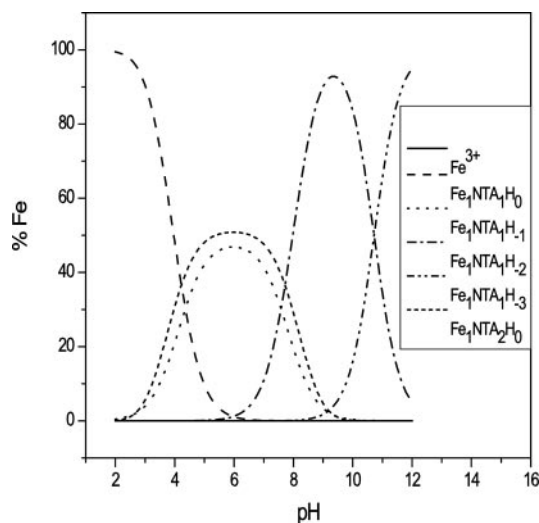


FIG. 1. Species distribution diagram for conditions found in ITC titrant (syringe) solution: 100 mM Hepes, pH 7.5, Fe:NTA present in 1:2 molar ratio.

solution characterized by ITC was adjusted to within ± 0.05 pH units); the concentration of NaHCO_3 , when present, was 25 mM.

For titrations performed in the absence of bicarbonate, 20 consecutive 5- μ l aliquots of 1.6 mM Fe-NTA (2-fold molar excess of NTA) in buffer were injected into the sample cell (volume = 1.3528 ml) containing 20 μ M mTf. The time between each injection was 5 min. To avoid contamination by CO_2 , the ITC sample cell and the injection syringe were flushed with pure nitrogen before filling.

For titrations performed in the presence of bicarbonate, 5- or 10- μ l aliquots of Fe-NTA were injected into the sample cell at intervals of 10–30 min. The tight binding of iron to mTf in the presence of bicarbonate precluded the determination of the binding constant by ITC for these systems; only binding enthalpies, ΔH_b , were measured.

Control experiments were performed by titrating Fe-NTA solution into protein-free buffer. To determine ΔC_p , the heat capacity change upon binding, ΔH_b was determined at several temperatures between 25 and 37 °C. The slope of a plot of ΔH_b versus temperature then provided ΔC_p under the assumption that it is temperature-independent over the relatively small temperature range of physiological relevance (20–40 °C). Samples were degassed before loading into the sample cell and injection syringe. Each ITC experiment was performed two to three times and the average binding parameters and associated error calculated.

Differential Scanning Calorimetry—DSC studies were performed on a MicroCal VP-DSC (MicroCal Inc.). All experiments were carried out in 500 mM Hepes, 25 mM NaHCO_3 , pH 7.5, at a scan rate of 60 °C/h. Background excess thermal power scans were obtained with buffer containing 0–15 mM Fe-NTA (1:2 molar ratio) in both the sample and reference cells and subtracted from the scans for each sample solution containing 1.5–2.0 mg/ml mTf and the same Fe-NTA concentration. All samples were degassed for 7 min with gentle stirring under vacuum prior to loading into the calorimeter. Reversibility of unfolding was determined by reheating the sample after cooling in the calorimeter. Data analysis was performed by fitting to the two-dimensional ligand binding model described elsewhere (23).

RESULTS

Isothermal Titration Calorimetry Studies of Bicarbonate-free System—In all isothermal titrations reported, an apo-mTf-containing sample cell was titrated with ferric ions present in solution in the form of an equilibrium set of $\text{Fe}_x\text{NTA}_y\text{H}_z$ complexes, where x , y , and z represent the stoichiometric coefficients for each complex present. Following the IUPAC speciation convention (24), negative values of z indicate the number of hydroxyl ions participating in the complex. Motekaitis and Martell (25) have measured an accurate set of equilibrium formation constants that can be used to compute chemical equilibria of aqueous solutions containing ferric ion and NTA over the pH range 2–10. Fig. 1 shows a $\text{Fe}_x\text{NTA}_y\text{H}_z$ complex speciation diagram over this pH range for the case where NTA

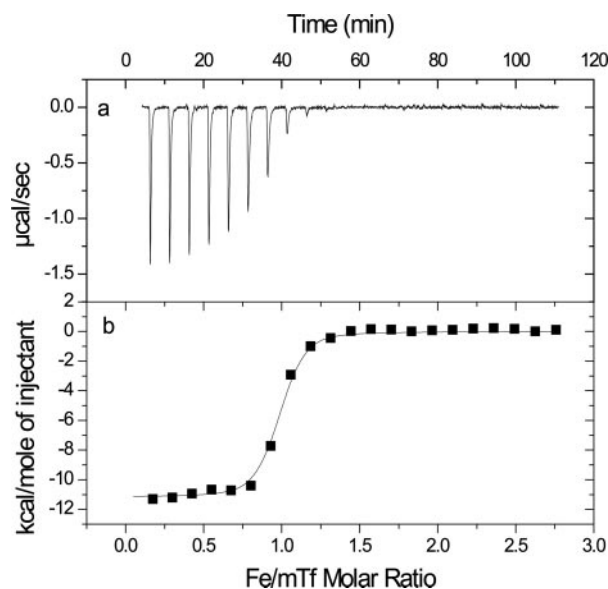


FIG. 2. Raw data (a) and integrated heat changes (symbols) fitted to one-site model (line) (b) for the ITC titration of 20 μM mTf with 0.65 mM Fe·NTA in 100 mM Hepes, pH 7.5, at 37 $^{\circ}\text{C}$.

is present in 2-fold molar excess relative to iron, the NTA:Fe concentration ratio used in all ITC experiments. At pH 7.5, iron is present in solution as a $\text{Fe}_1\cdot\text{NTA}_2\cdot\text{H}_0$ complex (41.1%), a $\text{Fe}_1\cdot\text{NTA}_1\cdot\text{H}_{-1}$ complex (32.2%), and a $\text{Fe}_1\cdot\text{NTA}_1\cdot\text{H}_{-2}$ complex (26.7%), with the concentration of free ferric ion ($\text{Fe}_1\cdot\text{NTA}_0\cdot\text{H}_0$) being vanishingly small in accordance with iron solubility data.

To simplify our remaining discussion of iron binding to mTf, we hereafter collectively refer to the equilibrium set of $\text{Fe}_x\cdot\text{NTA}_y\cdot\text{H}_z$ complexes in solution at reaction temperature and pH 7.5 as Fe·NTA. In all ITC experiments reported here, NTA and iron are loaded into the injection syringe in 2:1 molar ratio. Initially, the sample cell contains no iron or NTA. Raw ITC data for the titration at pH 7.5, 37 $^{\circ}\text{C}$, and no added synergistic bicarbonate anion show that Fe·NTA binds mTf (Fig. 2a) with a stoichiometry of one ferric ion bound/molecule of mTf. This differs from the well documented 2:1 iron-binding stoichiometry of other transferrins (oTf, hTf, and Lf) and supports the binding model proposed by Baker *et al.* (16) in which the C lobe of mTf is designated as incapable of binding iron due to the absence of appropriate ligands within the cleft formed at the junction of its two subdomains.

The dilution-corrected integrated heat response associated with each injection of Fe·NTA is plotted in Fig. 2b along with the best fit of a putative binding model that assumes that each molecule of mTf has a single type of site for binding a single type of ligand, assumed here to be the $\text{Fe}_1\cdot\text{NTA}_1\cdot\text{H}_0$ complex. As shown in Fig. 1, the ferric ion is present in a number of equilibrium complexes in solution at pH 7.5. Our assumption of a single type of ligand ($\text{Fe}_1\cdot\text{NTA}_1\cdot\text{H}_0$ complex) therefore implicitly assumes that equilibration of iron within the various $\text{Fe}_x\cdot\text{NTA}_y\cdot\text{H}_z$ complexes is rapid compared with uptake of the $\text{Fe}_1\cdot\text{NTA}_1\cdot\text{H}_0$ complex by mTf. The model is fit to the ITC data by regression (using summation of the squared residual errors and the Levenberg-Marquardt algorithm) of its three floating parameters. These model parameters include n , the number of ligand-binding sites/molecule of mTf, $K_{1,\text{app}}$, the apparent equilibrium association constant for ligand binding (M^{-1}), and ΔH_1 , the molar heat of binding (kcal/mol). Table I reports the best fit values of each model parameter for Fe·NTA binding to mTf at two different temperatures. The model fit to the data is excellent, and at both reaction temperatures n is near unity, supporting a 1:1 binding stoichiometry. $K_{1,\text{app}}$ is moderately strong

TABLE I

Results of model fit to ITC data for binding of Fe·NTA to mTf in the absence of bicarbonate, 100 mM Hepes, pH 7.5

n , number of ligand-binding sites/molecule of mTf. $K_{1,\text{app}}$, apparent equilibrium association constant for ligand binding. ΔH_1 , molar heat of binding.

| Temperature | n | ΔH_1 | $K_{1,\text{app}} \times 10^{-7}$ |
|--------------------|---------------------|---------------------|-----------------------------------|
| $^{\circ}\text{C}$ | | kcal/mol | |
| 25 | 0.92 (± 0.05) | -8.6 (± 0.4) | 2.6 (± 0.4) |
| 37 | 0.94 (± 0.05) | -11.1 (± 0.1) | 1.4 (± 0.1) |

(order 10^7 M^{-1}) and decreases with increasing temperature, in accordance with the exothermic peaks observed during the binding reaction. At 37 $^{\circ}\text{C}$, iron binding in the absence of bicarbonate is driven exclusively by enthalpy, as $T\Delta S$, the entropic contribution to binding, is near zero (-1 kcal/mol) at this temperature. This negligible overall change in entropy suggests that the inherent entropy loss in Fe·NTA upon binding to mTf is compensated for by concomitant dehydration effects that result in a net increase in solvent entropy. The temperature dependence of ΔH_1 gives an estimate of the heat capacity change $\Delta C_{p,1}$ for Fe·NTA binding of $\sim -200 \text{ cal/mol K}$.

Isothermal Titration Calorimetry Studies in the Presence of Bicarbonate—Raw ITC results for ferric ion binding to mTf in the presence of bicarbonate (Fig. 3) are considerably more complicated than observed for the bicarbonate-free system. At 37 $^{\circ}\text{C}$, injection of each of the first four aliquots of Fe·NTA into the mTf-containing sample cell results in a sharp exothermic peak immediately followed by an endothermic peak. An expanded view of the heat response following the first injection of Fe·NTA is shown in Fig. 4 to facilitate interpretation of results. The sign change of the heat response suggests that binding of Fe·NTA to the N lobe of mTf occurs in a series of at least two reaction subprocesses, the rates of which differ appreciably, when the synergistic bicarbonate anion is present. The first subprocess, characterized by the narrow exothermic peak at the start of the heat response, occurs over a time period shorter than the response time of the instrument. The second subprocess occurs more slowly and is characterized by a relatively broad endothermic peak. As the mTf becomes saturated with ferric ion, both peaks diminish in size (injections 3–5) until one observes only a single endothermic peak (injections 7–10) with a size and shape equal to the heat of dilution of Fe·NTA, indicating complete saturation of mTf.

Calorimetry studies of the binding of Fe·NTA to apo-oTf in the presence of bicarbonate are reported by Lin *et al.* (18). Heat responses observed for binding of the Fe·NTA complex to the N lobe of oTf are quite similar to those shown in Fig. 3 for Fe·NTA binding to mTf under the same conditions. They attribute the heat released in the initial sharp exothermic peak to a subprocess involving rapid binding, which they term “contact binding,” of the Fe·NTA complex to the binding cleft of the N lobe of oTf. As in our experiments on mTf, contact binding of oTf occurs rapidly and is strongly exothermic. Lin *et al.* attribute the second step, for which (as in our case) the reaction kinetics are considerably slower than observed for the contact binding step, to insertion of the synergistic bicarbonate anion and concomitant release of NTA from the bound Fe·NTA complex. Certain details of this proposed bicarbonate insertion mechanism are problematic as, at the very least, the bound bicarbonate anion must work in concert with at least 2 of the amino acid ligands provided by oTf to establish a net favorable energetic driving force for NTA displacement. However, these small errors do not in any significant way detract from the modeling of the ITC heat response data of Lin *et al.* in terms of a rapid contact binding step followed by a kinetically controlled NTA displacement step. Moreover, the strong similarity of our ITC

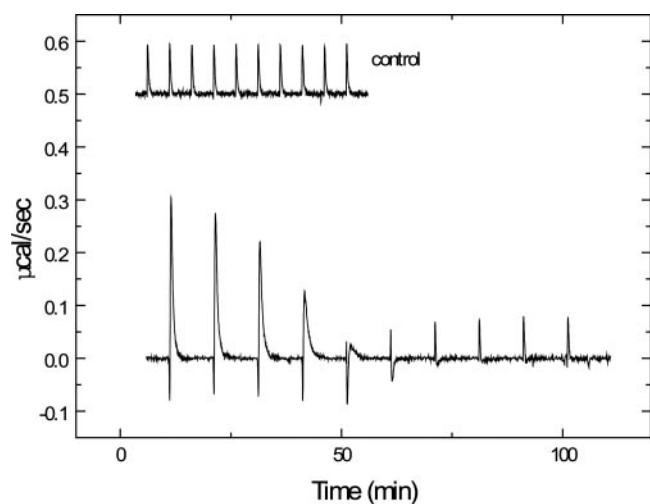


FIG. 3. Raw data for ITC titration of 17 μM mTf with 0.8 mM Fe-NTA in 100 mM Hepes, 25 mM NaHCO_3 , pH 7.5, at 37 $^\circ\text{C}$. The control titration is performed by titrating 0.8 mM Fe-NTA into protein-free buffer.

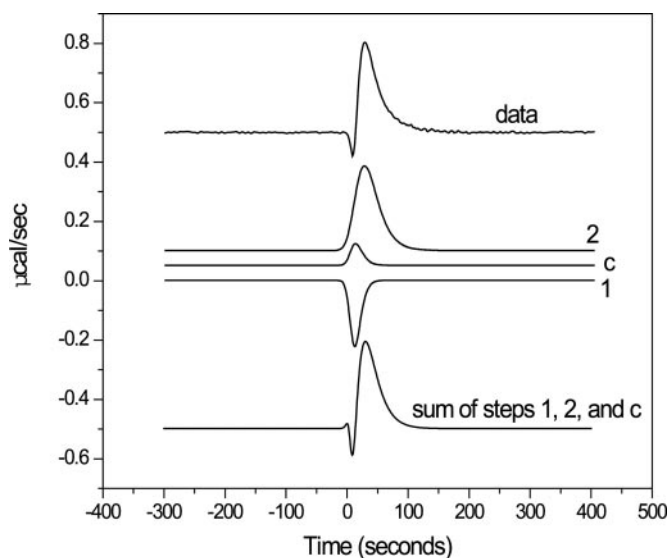


FIG. 4. Deconvolution of the first peak for ITC titration of 17 μM mTf with 0.8 mM Fe-NTA in 100 mM Hepes, 25 mM NaHCO_3 , pH 7.5, at 37 $^\circ\text{C}$ given in Fig. 3. Simulated peaks are shown for the subprocesses of contact binding (*step 1*), NTA release and domain closure (*step 2*), and heat of dilution of Fe-NTA (*c*).

results (Fig. 3) with those reported by Lin *et al.* for the N lobe of oTf provides further compelling evidence that mTf binds a single ferric ion at its N lobe with no iron binding at its C lobe.

Our ITC results were analyzed with respect to the crystallographic data of Kuser *et al.* (26) by deconvoluting each of the heat responses to obtain peak shapes and areas for the three contributing steps in ferric ion binding to mTf in the presence of bicarbonate. An example of this deconvolution process is given in Fig. 4. *Peak c* is the control peak defining the heat of dilution of Fe-NTA. *Peak 1* provides an estimate of the heat released during contact binding of the Fe-NTA complex. *Peak 2* is an estimate of the endotherm due to gradual displacement of NTA in the bound Fe-NTA complex with ligands provided first by Tyr-188 and then by His-249 and Tyr-95 and the ligation of Asp-63 with the concomitant closing of the binding cleft. Standard enthalpies for each step in the binding reaction, estimated from the area of the associated peaks, are listed in Table II along with the standard apparent total enthalpy change

TABLE II

Standard enthalpies for each step in the binding reaction of Fe-NTA to mTf in the presence of bicarbonate (25 mM), 100 mM Hepes, pH 7.5 at 37 $^\circ\text{C}$, estimated from the areas of the peaks shown in Fig. 4

| ΔH_1 | ΔH_2 | $\Delta H_{b,\text{app}}$ | $\Delta C_{p,b}$ |
|--------------|--------------|---------------------------|------------------|
| | | <i>kcal/mol</i> | |
| -2.4 | 8.7 | 6.3 | -350 |

($\Delta H_{b,\text{app}} = \Delta H_1 + \Delta H_2$) and overall heat capacity change $\Delta C_{p,b}$ for the binding reaction.

The slow kinetics of step 2 of NTA-complexed ferric ion binding to mTf indicates that equilibrium may not be reached over the duration of each titration experiment. As a result, the accuracy of an apparent equilibrium constant for ferric ion binding to mTf in the presence of bicarbonate regressed from ITC data is uncertain and therefore not presented here.

DSC Studies of Ferric Ion Binding to mTf in the Presence of Bicarbonate—For apo-mTf in a pH 7.5 solution containing 25 mM NaHCO_3 , Fig. 5 shows the DSC thermogram after subtraction of the protein-free buffer baseline scan and normalization with protein concentration. Rescans of the sample show that the thermal unfolding of mTf is more than 70% reversible at the solution conditions (500 mM HEPES buffer) and scan rate (60 $^\circ\text{C}/\text{h}$) used. As will be verified in DSC thermograms of mTf in the presence of ferric ion, the unfolding thermogram of apo-mTf is the sum of three unfolding transitions, each of which can be described by the two-state transition model. The two-state model fit of each contributing transition is shown in Fig. 5 (*dotted lines*) with the largest peak corresponding to the thermal denaturation of the N lobe of apo-mTf. Although the N lobe is composed of two conformationally distinct subdomains (N1 and N2), the melting transitions of these two subdomains are tightly linked, such that their melting temperatures overlap and their combined melting envelope can be modeled as a single two-state transition. A similar observation is made by Lin *et al.* (21) in their DSC studies of hTf, which show that the melting transitions of the N and C lobes can each be described by a single two-state transition peak. However, this simplifying assumption is not valid for the two subdomains of the C lobe of mTf. The two small peaks in Fig. 5 represent the two-state model fits of the melting transitions for the C1 and C2 subdomains of the C lobe of mTf. As the C lobe is unique in its inability to bind iron, our results suggest that tight linkage of the melting transitions of the N lobe subdomains of mTf is a requirement for their iron binding function, which requires the precise coordination of the N1 and N2 subdomains and the two β -strands comprising the lobe hinge to properly position the four required iron binding ligands. As the C lobe does not bind iron, tight coupling of subdomain melting temperatures is no longer required.

Transition enthalpies ΔH_{N-U} and melting temperatures T_m regressed from the fitting of the two-state model to the unfolding thermogram for apo-mTf are shown in Table III. The total calorimetric heat ΔH_{cal} for the unfolding of apo-mTf, obtained by integration of the experimental thermogram, is 367.5 kcal/mol. The sum of the ΔH_{N-U} values given by the areas of the three contributing thermal transitions is 354 ± 32 kcal/mol, in close agreement with ΔH_{cal} . As one might expect from their relatively high degree of sequence homology, the two lobes of mTf contribute nearly equally (173 and 181 kcal/mol for the N and C lobes, respectively) to the observed ΔH_{cal} for mTf.

The overlap of the three contributing melting transitions does not permit determination of the heat capacity change $\Delta C_{p,N-U}$ associated with each unfolding transition. However, the total heat capacity change for the thermal unfolding of mTf can be determined, having a value of 6 kcal/mol K based on

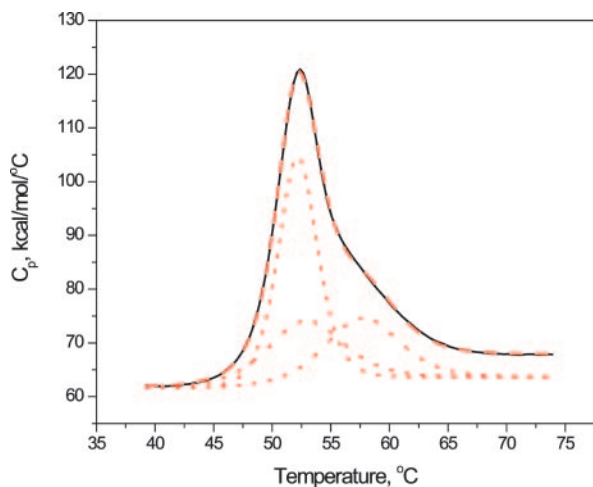


FIG. 5. DSC thermogram of apo-mTf in 500 mM Hepes, 25 mM NaHCO₃, pH 7.5 (solid line) with fit to two-state model (dashed line) including three independent domains (dotted lines).

TABLE III
Two-state fit results of DSC thermograms for apo-mTf in 25 mM bicarbonate, 500 mM Hepes, pH 7.5

| Model | T _m °C | ΔH _{N-U} kcal/mol | ΔC _{p,N-U} ^a |
|--------------|----------------------|-------------------------------|----------------------------------|
| 3-Domain fit | | | |
| Peak 1 | 52.2 (± 0.2) | 173 (± 9) | 3 |
| Peak 2 | 53.2 (± 0.7) | 84 (± 17) | 1.5 |
| Peak 3 | 56.9 (± 0.9) | 97 (± 6) | 1.5 |

^a ΔC_{p,N-U} values were fixed during the fit.

global regression of the average baseline shift in four independent DSC thermograms. Additional lobe-specific thermodynamic information can be calculated by assuming that the N and C lobes of mTf contribute equally (3 kcal/mol K each) to the observed overall heat capacity change, that the C1 and C2 subdomains contribute equally (1.5 kcal/mol K each) to the ΔC_{p,N-U} for the C lobe, and that all reported ΔC_p values are temperature-independent.

Fig. 6 shows DSC thermograms of mTf in the presence of iron at concentrations up to 100 times the mTf concentration. Through mass action effects (*i.e.* Le Chatelier's principle), the equilibrium between the native and denatured states is shifted strongly toward the native state because the ferric ion can only bind to the N lobe of mTf in its native state conformation. Addition of Fe-NTA therefore increases the T_m of the N lobe by more than 30 °C, resulting in the appearance of a thermal transition at 82.4 °C and the concomitant disappearance of the thermal transition observed for the apo-N lobe at 52.1 °C.

The addition of Fe-NTA has a much smaller effect on the melting temperatures of the two C lobe subdomains of mTf, consistent with the inferred inability of the C lobe to bind iron. For the C lobe subdomain characterized by a T_m in the apo-state of 53.2 °C, no change in T_m is observed with increasing loading of Fe-NTA. The T_m for the second subdomain does increase but only by 2.3 °C when mTf becomes saturated with iron. This modest change in stability is inconsistent with ligand binding to the subdomain and instead suggests an interlobe interaction through which the conformation and thermal stability of the C lobe are influenced by changes in the conformation and stability of the N lobe that accompany iron binding to the N lobe. For both hTf and oTf, interactions between the two lobes composing each protein have been shown to alter the conformation and increase the stability of iron-free lobe within the monoferric protein (21). The existence of a similar stabilization effect in mTf is therefore expected.

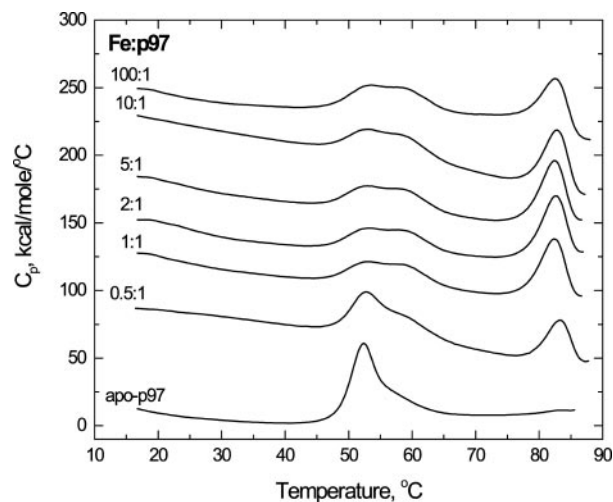


FIG. 6. DSC thermograms of mTf in the presence of Fe-NTA at various molar ratios of Fe to mTf, as indicated, in 500 mM Hepes, 25 mM NaHCO₃, pH 7.5.

The change in Gibbs energy ΔG_{N-C} stabilizing the C lobe of mTf as a result of its interaction with the N lobe can be estimated from the general thermodynamic relation as shown in Equation 1,

$$\Delta G_{N-C}(T_m^*) = \Delta H_{N-U,i} \left(1 - \frac{T_m^*}{T_m} \right) + \Delta C_{p,i} \left(T_m^* \ln \frac{T_m}{T_m^*} + T_m^* - T_m \right) \quad (\text{Eq. 1})$$

where T_m and T_m^{*} are the melting temperatures of subdomain C1 for apo- and holo-mTf, respectively. The origins of Equation 1 are fully described by Brandts *et al.* (27). Saturation of mTf shifts the T_m of the two-state transition peak for C2 from 56.9 °C (apo-mTf) to 59.3 °C (holo-mTf), giving a value of ΔG_{N-C} of -0.72 kcal/mol. This stabilization energy is appreciably smaller than that observed for oTf where the ΔG_{N-C} stabilizing the C lobe due to preferential iron binding to the N lobe was estimated to be -3.1 kcal/mol (21). Similarly, the N lobe of hTf is stabilized by a ΔG_{C-N} of -3.0 kcal/mol, indicating the need for much stronger allosteric coupling in transferrins capable of binding a ferric ion at each lobe.

The apparent equilibrium constant K_{app} for binding of a ferric ion, presented in solution as an equilibrium distribution of Fe_xNTA_yH_z chelation complexes, can be estimated through application of the equations for the unfolding of a protein in the presence of a ligand that binds only to the native-state conformation of the protein (23, 28). In addition to the DSC data shown in Fig. 6, the analysis requires knowledge of the change in enthalpy ΔH_b and heat capacity ΔC_{p,b} for the ligand binding reaction. Both values were determined from ITC data for iron binding to mTf in the presence of 25 mM NaHCO₃ over the temperature range 20–40 °C; ΔH_b (25 °C) = 10.5 kcal/mol and ΔC_{p,b} = -350 cal/mol⁻¹ K⁻¹ and is assumed to be temperature-independent. Application of the theory (23) then gives an estimate of K_{app} of 4.4 °C × 10¹⁷ M⁻¹ at 25 °C and 7.6 × 10¹⁷ M⁻¹ at 37 °C for binding of the ferric ion to the N lobe of mTf in the presence of bicarbonate.

DISCUSSION

Ferric binding to mTf in the presence of bicarbonate is accompanied by a large negative change in heat capacity similar in magnitude to that found for oTf and hTf (18, 19). Although many factors can contribute to ΔC_{p,b}, negative values observed for binding reactions in aqueous solvent environments are generally associated with the dehydration of apolar surfaces, such as hydrophobic amino acids (29). However, the transferrin

binding clefts are hydrophilic, as they are generally comprised of many polar side chains and contain 10–20 tightly associated H₂O molecules (15). The negative $\Delta C_{p,b}$ for mTf is therefore likely attributed to conformational changes in the protein to a more compact, less solvated structure upon binding of ferric ion, as has been argued for iron binding to hTf and oTf (18, 19). This change in conformation is supported by x-ray crystallographic structures of hTf, oTf, and Lf (15, 30).

In particular, it is useful to draw comparisons with available crystal structure data for the related protein oTf in both its apo and holo states. For duck oTf, Kuser *et al.* (26) show that the synergistic bicarbonate anion binds to the N terminus of helix 5 on the N lobe of apo-oTf through a network of hydrogen bonds formed with OG1 of Thr-120 (all amino acids designated according to hTf numbering), the main chain NH groups of Ala-126 and Gly-127, and the guanidinium group of Arg-124. The bicarbonate anion therefore retains in its bound state two free oxygen ligands to the metal. Dewan *et al.* (30) found that the two β -strands that connect subdomains N1 and N2 of the N lobe of hen oTf act as a hinge to open or close the iron binding interfacial cleft formed by the contact of the two subdomains. In the absence of bound iron, the hinge is open and the cleft solvent exposed. In holo-oTf, the ferric ion bound within the N lobe is ligated to 4 amino acid side chains on residues that are remote from one another on the protein sequence. Each of the two β -strands comprising the lobe hinge provides 1 of these 2 amino acids, Tyr-95 and His-249. The remaining 2 amino acids, Asp-63 and Tyr-188, are provided by subdomains N1 and N2, respectively.

X-ray diffraction data from both Dewan *et al.* (30) and Kuser *et al.* (26) suggest that oTf preferentially binds the Fe₁-NTA₁-H₀ complex. NTA forms this tetradentate complex with the high spin ferric ion through its three carboxyl groups and central nitrogen. oTf binds the Fe₁-NTA₁-H₀ complex through a stepwise process that begins with binding of the ferric ion through formation of a bidentate complex with the prebound bicarbonate anion and ligation to Tyr-188, resulting in the displacement of the two water ligands. Immediately following this “contact binding” step (step 1), the Fe-NTA complex slowly dissociates as evidenced by an increase in separation distances of the Fe-O12(NTA) and Fe-N(NTA) ligand interactions (step 2). Although strengthening of the Fe:HCO⁻³ chelate may contribute, NTA dissociation appears to require ligand exchange with His-249 and the second tyrosine, Tyr-95, which properly coordinate with the octahedral coordination sphere of the ferric ion as the N lobe subdomain hinge begins to close. Complete dissociation and removal of the NTA ligand then allows further closure of the binding cleft, allowing Asp-63 in domain N1 to occupy the remaining coordination site. Because Asp-63 is the only ligand from the N1 domain and it also forms an important interdomain hydrogen bond, Grossmann *et al.* (31) have argued that most of the observed conformational change in the N lobe coincides with the ligation of this final residue to the bound ferric ion. A similar domain closure in mTf is expected to occur during iron binding in the presence of bicarbonate.

In the absence of bicarbonate the $\Delta C_{p,b}$ remains negative, although not as large. This smaller change in $\Delta C_{p,b}$ is attributable to removal of fewer solvating water molecules when bicarbonate is not present, resulting in a less compact structure when iron binds to mTf. In addition, NTA may not dissociate from iron if bicarbonate is not present. Maintenance of the Fe-NTA complex in the binding pocket may also contribute to a more open structure.

The apparent binding constant for Fe-NTA to mTf in the presence of bicarbonate determined from the series of DSC

thermograms at various Fe-mTf ratios is $4.4 \times 10^{17} \text{ M}^{-1}$ at 25 °C. Under the same conditions, Lin *et al.* (21) determined K_{app} to be 1.5×10^{18} and $1.5 \times 10^{14} \text{ M}^{-1}$ for the N and C sites, respectively, of oTf, and 1.1×10^{22} and $8 \times 10^{13} \text{ M}^{-1}$ for the corresponding sites of hTf. These values may represent overestimates of K_{app} , and thus K the binding constant of iron to Tf in the absence of chelator, because the T_m values were controlled by kinetic factors at the scan rates used in the DSC experiments, *i.e.* the unfolding reaction at the true T_m is too slow relative to the scan rate to be observed. The same kinetic effects are observed in the case of mTf, suggesting that the observed K_{app} of $4.4 \times 10^{17} \text{ M}^{-1}$ may represent an overestimate of the true value. As a result, the relative values of K_{app} are likely more informative than the absolute values. We observe that the apparent binding constant of iron to mTf obtained by DSC is similar in magnitude to that observed by DSC for hTf and oTf and falls in a range between K_{app} for the N and C lobes of hTf. Although the function of soluble mTf is unknown, it is believed to relate in some way to iron storage and transport (15). The fact that its affinity for iron is intermediate between the two lobes of hTf may therefore provide a clue to its function in the body.

It is not known why organisms need an alternate to the TfTfR pathway for iron uptake. Although there are many examples of specific uptake of non-Tf bound iron (NTBI) into cell types (1), little is known about the molecules involved in these processes. These experiments have shown that both high and low affinity mechanisms ($K_m = 0.5\text{--}20 \mu\text{M}$) are involved in NTBI uptake. In addition, these alternate iron uptake processes are energy-dependent and are not regulated by the level of iron in the cell (32). Furthermore, it is suggested that the uptake of NTBI might play a role in iron overload in diseases such as hemochromatosis and other iron overload disorders (33). Our data show that mTf may provide another mechanism for cells to acquire iron. It is also possible that GPI-anchored p97 provides essential iron to the cells when the TfTfR system is absent, as is the case in hypotransferrinemic mice (34). The observation that these mice can take up large amounts of dietary iron and become iron overloaded despite the lack of serum Tf suggests that the non-Tf-bound iron mechanisms are likely responsible for delivering iron into the tissues resulting in iron overload (35). GPI-anchored p97 has been shown to localize to the apical side of fetal intestine (13, 36), whereas TfR is mainly found on the basal-lateral side of such cells. This would suggest a possible function for GPI-anchored p97 in intestinal iron uptake. Our results suggest that at normal pH and salt concentrations p97 binds a single atom (37). In addition, the N lobe of p97 binds iron with a higher affinity than that of the C lobe of Tf (37). It is therefore interesting that it was recently demonstrated that upon binding of Tf to TfR, a conformation change occurs in Tf that hinders the release of iron from the N lobe of Tf, suggesting perhaps only one atom of iron is released within the cell during each round of internalization (6). Given that mammalian cells in culture may express $\sim 1.0 \times 10^6$ molecules of p97/cell (7), the efficiency of iron uptake via p97 may thus rival that of the classical TfTfR pathway. Thus it is intimated from the estimated K_{app} of $4.4 \times 10^{17} \text{ M}^{-1}$ for mTf that the soluble form of mTf likely has a role in iron transport in tissues where hTf is in low concentrations or where the N lobe of hTf is otherwise occupied by iron. Understanding where these anatomical and physiological conditions exist is the next challenge.

Acknowledgments—We thank Soren Jensen and Michelle Yee for assistance in the DSC experiments and Nooshafarin Sanaie for multiple chemical equilibrium calculations.

REFERENCES

1. Wessling-Resnick, M. (2000) *Annu. Rev. Nutr.* **20**, 129–151
2. Andrews, N. C. (2000) *Annu. Rev. Genomics Hum. Genet.* **1**, 75–98
3. Donovan, A., Brownlie, A., Zhou, Y., Shepard, J., Pratt, S. J., Moynihan, J., Paw, B. H., Drejer, A., Barut, B., Zapata, A., Law, T. C., Brugnara, C., Lux, S. E., Pinkus, G. S., Pinkus, J. L., Kingsley, P. D., Palis, J., Fleming, M. D., Andrews, N. C., and Zon, L. I. (2000) *Nature* **403**, 776–781
4. Fleming, M. D., Romano, M. A., Su, M. A., Garrick, L. M., Garrick, M. D., and Andrews, N. C. (1998) *Proc. Natl. Acad. Sci. U. S. A.* **95**, 1148–1153
5. Gunshin, H., Mackenzie, B., Berger, U. V., Gunshin, Y., Romero, M. F., Boron, W. F., Nussberger, S., Gollan, J. L., and Hediger, M. A. (1997) *Nature* **388**, 482–488
6. Cheng, Y., Zak, O., Aisen, P., Harrison, S. C., and Walz, T. (2004) *Cell* **116**, 565–576
7. Kennard, M. L., Richardson, D. R., Gabathuler, R., Ponka, P., and Jefferies, W. A. (1995) *EMBO J.* **14**, 4178–4186
8. Rose, T. M., Plowman, G. D., Teplow, D. B., Dreyer, W. J., Hellstrom, K. E., and Brown, J. P. (1986) *Proc. Natl. Acad. Sci. U. S. A.* **83**, 1261–1265
9. Woodbury, R. G., Brown, J. P., Yeh, M. Y., Hellstrom, I., and Hellstrom, K. E. (1980) *Proc. Natl. Acad. Sci. U. S. A.* **77**, 2183–2187
10. Rothenberger, S., Food, M. R., Gabathuler, R., Kennard, M. L., Yamada, T., Yasuhara, O., McGeer, P. L., and Jefferies, W. A. (1996) *Brain Res.* **712**, 117–121
11. McNagny, K. M., Rossi, F., Smith, G., and Graf, T. (1996) *Blood* **87**, 1343–1352
12. Food, M. R., Rothenberger, S., Gabathuler, R., Haidl, I. D., Reid, G., and Jefferies, W. A. (1994) *J. Biol. Chem.* **269**, 3034–3040
13. Alemany, R., Vila, M. R., Franci, C., Egea, G., Real, F. X., and Thomson, T. M. (1993) *J. Cell Sci.* **104**, Pt. 4, 1155–1162
14. Moroo, I., Ujiie, M., Walker, B. L., Tiong, J. W., Vitalis, T. Z., Karkan, D., Gabathuler, R., Moise, A. R., and Jefferies, W. A. (2003) *Microcirculation* **10**, 457–462
15. Baker, H. M., Anderson, B. F., and Baker, E. N. (2003) *Proc. Natl. Acad. Sci. U. S. A.* **100**, 3579–3583
16. Baker, E. N., Rumball, S. V., and Anderson, B. F. (1987) *Trends Biochem. Sci.* **12**, 350–353
17. Aisen, P., Leibman, A., and Zweier, J. (1978) *J. Biol. Chem.* **253**, 1930–1937
18. Lin, L. N., Mason, A. B., Woodworth, R. C., and Brandts, J. F. (1991) *Biochemistry* **30**, 11660–11669
19. Lin, L. N., Mason, A. B., Woodworth, R. C., and Brandts, J. F. (1993) *Biochemistry* **32**, 9398–9406
20. Lin, L. N., Mason, A. B., Woodworth, R. C., and Brandts, J. F. (1993) *Biochemistry* **32**, 9398–9406
21. Lin, L. N., Mason, A. B., Woodworth, R. C., and Brandts, J. F. (1994) *Biochemistry* **33**, 1881–1888
22. Baker, E. N., Baker, H. M., Smith, C. A., Stebbins, M. R., Kahn, M., Hellstrom, K. E., and Hellstrom, I. (1992) *FEBS Lett.* **298**, 215–218
23. Creagh, A. L., Koska, J., Johnson, P. E., Tomme, P., Joshi, M. D., McIntosh, L. P., Kilburn, D. G., and Haynes, C. A. (1998) *Biochemistry* **37**, 3529–3537
24. Martell, A. E., and Smith, R. M. (1974) *Critical Stability Constants*, Plenum Press, New York
25. Motekaitis, R. J., and Martell, A. E. (1994) *J. Coord. Chem.* **31**, 67–78
26. Kuser, P., Hall, D. R., Haw, M. L., Neu, M., Evans, R. W., and Lindley, P. F. (2002) *Acta Crystallogr. Sect. D Biol. Crystallogr.* **58**, 777–783
27. Brandts, J. F., Hu, C. Q., Lin, L. N., and Mos, M. T. (1989) *Biochemistry* **28**, 8588–8596
28. Brandts, J. F., and Lin, L. N. (1990) *Biochemistry* **29**, 6927–6940
29. Gomez, J., Hilser, V. J., Xie, D., and Freire, E. (1995) *Proteins* **22**, 404–412
30. Dewan, J. C., Mikami, B., Hirose, M., and Sacchettini, J. C. (1993) *Biochemistry* **32**, 11963–11968
31. Grossmann, J. G., Mason, A. B., Woodworth, R. C., Neu, M., Lindley, P. F., and Hasnain, S. S. (1993) *J. Mol. Biol.* **231**, 554–558
32. Gutierrez, J. A., Inman, R. S., Akompong, T., Yu, J., and Wessling-Resnick, M. (1998) *J. Cell. Physiol.* **177**, 585–592
33. McNamara, L., MacPhail, A. P., Mandishona, E., Bloom, P., Paterson, A. C., Rouault, T. A., and Gordeuk, V. R. (1999) *J. Gastroenterol. Hepatol.* **14**, 126–132
34. Takeda, A., Devenyi, A., and Connor, J. R. (1998) *J. Neurosci. Res.* **51**, 454–462
35. Buys, S. S., Martin, C. B., Eldridge, M., Kushner, J. P., and Kaplan, J. (1991) *Blood* **78**, 3288–3290
36. Danielsen, E. M., and van Deurs, B. (1995) *J. Cell Biol.* **131**, 939–950
37. Tiong, J. W. C. (2001) *The Iron (III) and Iron (II) Complexes of Nitrilotriacetic Acid*. Ph.D. thesis, University of British Columbia